

## Supplementary Information

### **Kosmotropic aqueous processing solution for green lithium battery cathode manufacturing**

Jung-Hui Kim<sup>1,†</sup>, Won-Yeong Kim<sup>1,†</sup>, Sebin Kim<sup>2,†</sup>, Jeongdong Kim<sup>1</sup>, Seok-Ju Lee<sup>1</sup>, Namjun Park<sup>2</sup>,  
Sun-Phil Han<sup>3</sup>, Kun Ryu<sup>4</sup>, Junghwan Kim<sup>1</sup><sup>✉</sup>, Won Bo Lee<sup>2</sup><sup>✉</sup>, Sang-Young Lee<sup>1,5</sup><sup>✉</sup>

<sup>1</sup>Department of Chemical and Biomolecular Engineering, Yonsei University, Seoul 03722, Republic of Korea

<sup>2</sup>School of Chemical and Biological Engineering, Institute of Chemical Processes, Seoul National University, Seoul 08826, Republic of Korea

<sup>3</sup>UNIST Central Research Facilities, Ulsan National Institute of Science and Technology (UNIST), Ulsan 44919, Republic of Korea

<sup>4</sup>Pritzker School of Molecular Engineering, The University of Chicago, Chicago, IL, USA

<sup>5</sup>Department of Battery Engineering, Yonsei University, Seoul 03722, Republic of Korea

<sup>†</sup>These authors contributed equally to this work: Jung-Hui Kim, Won-Yeong Kim, Sebin Kim

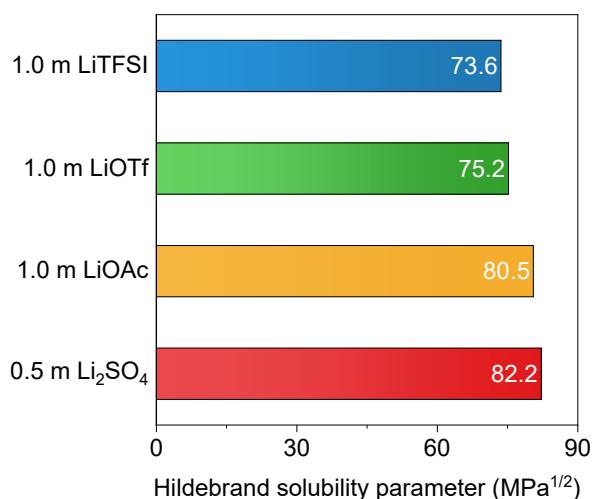
<sup>✉</sup>email: [kjh24@yonsei.ac.kr](mailto:kjh24@yonsei.ac.kr); [wblee@snu.ac.kr](mailto:wblee@snu.ac.kr); [syleek@yonsei.ac.kr](mailto:syleek@yonsei.ac.kr)

## Supplementary Figures



Supplementary Fig. 1 | Green scores of representative solvents. 5 criteria (Environmental Impact,

Health, Flammability & Explosion, Reactivity & Stability, and Life Cycle Assessment) were analyzed based on the GlaxoSmithKline (GSK) solvent selection guide<sup>1</sup>. Each of the evaluation factors has a score ranging from 0 to 10, with higher scores meaning better.



**Supplementary Fig. 2 | Hildebrand solubility parameter ( $\delta$ ) values of the electrolytes.** The values are calculated using the molecular dynamics (MD) trajectory.

#### **Supplementary Note 1 | Computational analysis method.**

To investigate the effects of anions in aqueous processing solutions, we conducted MD and DFT simulations. MD simulations predict the movement of molecules to describe the behavior of particles, while DFT calculates the electron density of molecules based on quantum mechanics. Therefore, MD simulations can be used to understand the properties of the system composed of electrolytes and NCM811, while DFT can be used to calculate the ESP of molecules or ions.

All MD simulations were performed using the GROMACS<sup>2</sup> molecular dynamics simulation package using optimized potentials for liquid simulation-all-atom (OPLS-AA) force field parameters. Force field parameters for OTf<sup>-</sup> and OAc<sup>-</sup> anions were generated by the LigPargen force field generator<sup>3</sup>. Parameters for other ions and water were taken from previous studies<sup>4-6</sup>. For a more accurate simulation of high polarizable aqueous electrolytes, the charges of all ions were scaled<sup>6</sup> to a factor of 0.85. In all runs, the integration timestep was 2 fs. Bond lengths for hydrogen bonds were constrained by the LINCS algorithm for most of the systems. For systems containing SO<sub>4</sub><sup>2-</sup> anions, the SHAKE algorithm was used. The cutoff distance was fixed at 12 Å for both short-range van der Waals and coulombic interactions. Long-range electrostatic interactions further than the cutoff distance were



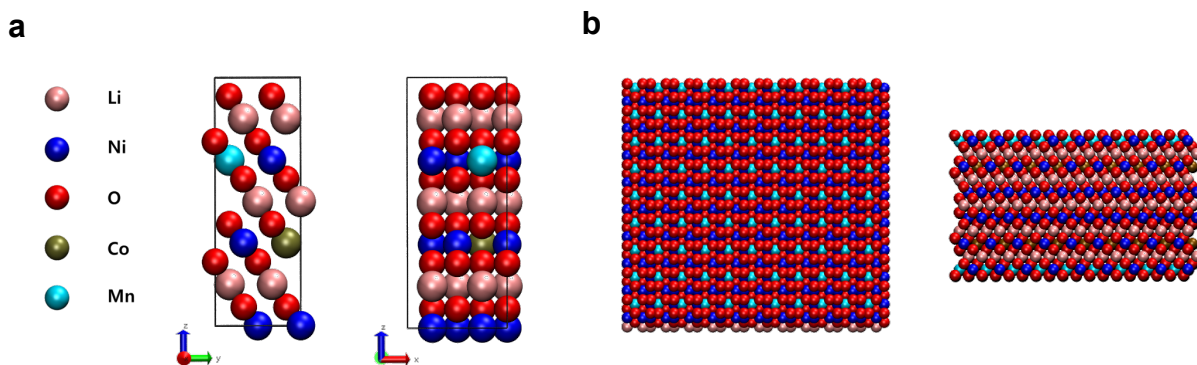
evaluated by the particle mesh Ewald (PME) method. Nosé-Hoover thermostat and Parinello-Rahman pressure coupling were used in MD simulations.

Hydrogen bonds were identified based on the geometric criterion that the distance between donor and acceptor atom was less than 3.5 Å and the angle between donor, hydrogen, and receptor was more than 150°. The Hildebrand solubility parameter ( $\delta$ ) was calculated from the following equation (1).

$$(1) \quad \delta = [(\Delta H_v - RT)/V_m]^{1/2} = \sqrt{CED}$$

$\delta$  denotes hildebrand solubility parameter,  $\Delta H_v$  denotes heat of vaporization, T denotes absolute temperature,  $V_m$  denotes molar volume and CED is cohesive energy density of the system.

The kosmotropic electrolyte with  $\text{SO}_4^{2-}$  showed higher  $\delta$  values (82.2  $\text{MPa}^{1/2}$ ) than those of other anions ( $\text{TFSI}^-$ : 73.6  $\text{MPa}^{1/2}$ ,  $\text{OTf}^-$ : 75.2  $\text{MPa}^{1/2}$ , and  $\text{OAc}^-$ : 80.5  $\text{MPa}^{1/2}$ ), despite half the concentration of  $\text{SO}_4^{2-}$ . This result suggests that strong kosmotropic anions can induce a high cohesive energy and effectively construct the more ordered hydration clusters.

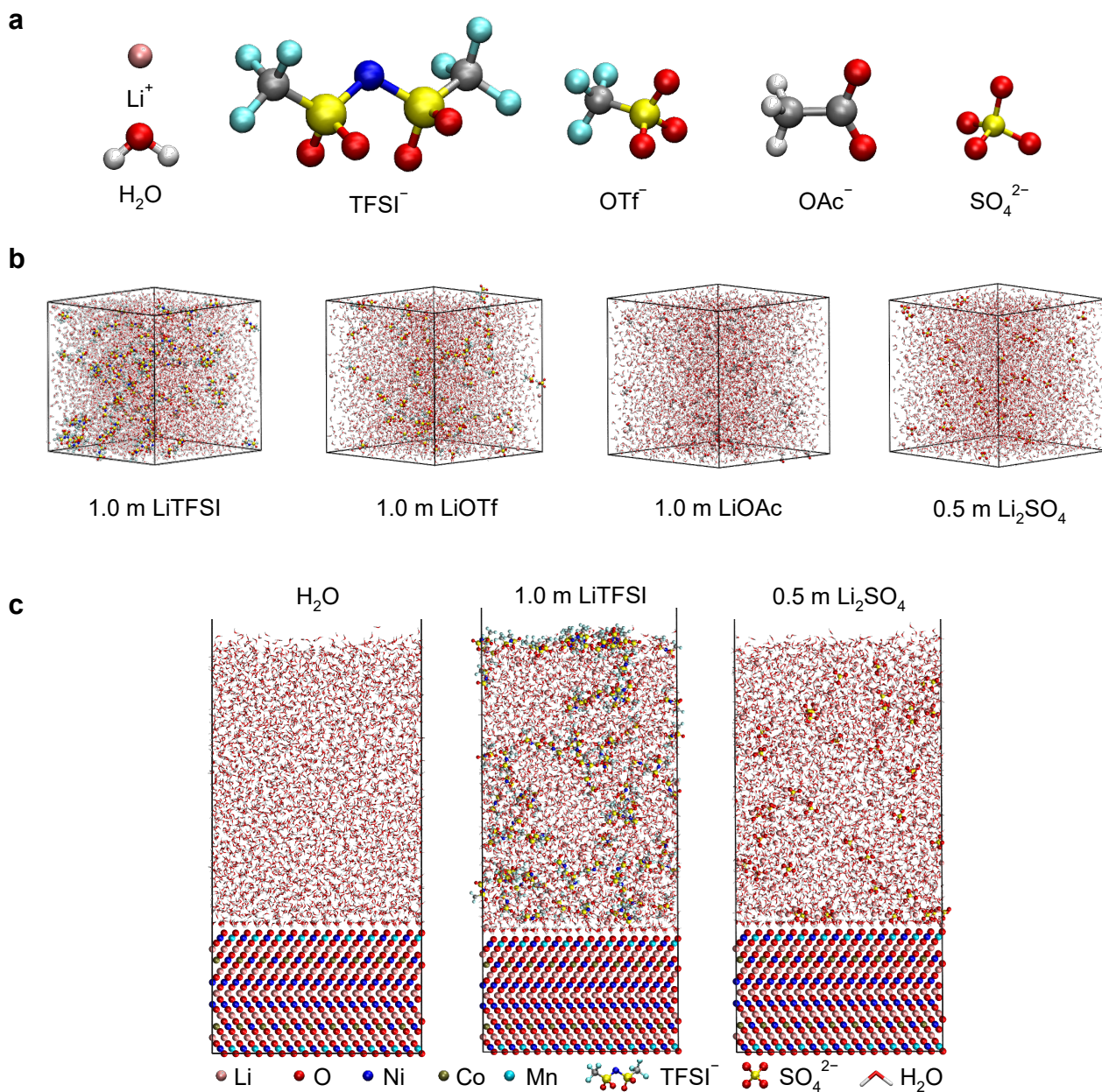


**Supplementary Fig. 3 | Simulated structure of NCM811 cathode materials.** a,b, The snapshots (left: top view, right: side view) of Ni-rich  $\text{LiNi}_{0.8}\text{Co}_{0.1}\text{Mn}_{0.1}\text{O}_2$  (NCM811) cathode materials: Unit cell (a), NCM811 film (b).

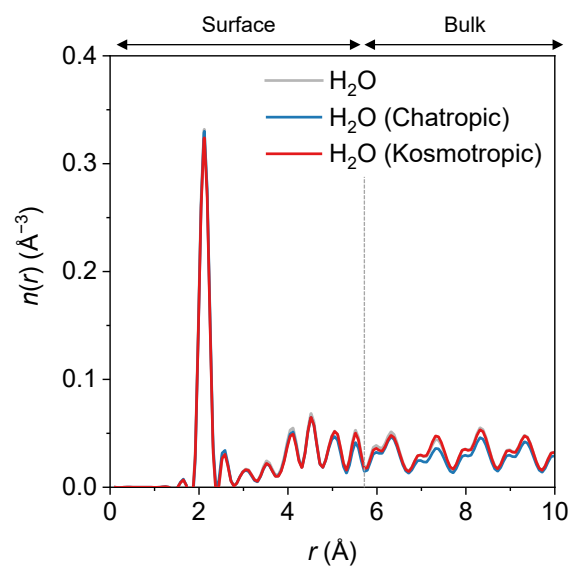
**Supplementary Note 2 | Detailed information on simulation of NCM811 cathode materials.**

To represent the NCM811 cathode, the atomic structure was manufactured based on the rhombohedral layered oxide structure (R-3m) of  $\text{LiNiO}_2$  (Inorganic Crystal Structure Database (ICSD) ID: 10499). The exact formula for the NCM811 used in this study is  $\text{Li}_{12}\text{Ni}_{10}\text{Co}_1\text{Mn}_1\text{O}_{24}$ , which was developed in the previous study<sup>7</sup>. Co and Mn, respectively, have replaced Ni atoms in a different slab of  $2 \times 2 \times 3$  supercell of  $\text{LiNiO}_2$  unit cell. For the convenience of molecular dynamics simulation, it was manufactured in a cubic cell, which is shown in **Supplementary Fig. 3a, Supplementary Data 1 and 2**. Based on the Li layer perpendicular to the z-axis inside the NCM811 unit cell, the remaining layers of the unit cell were symmetrically stacked in the z-axis to make the z-symmetric unit cell. The z-symmetric tNCM811 unit cell has no net dipole moment. For MD simulations, the  $11 \times 9 \times 1$  supercell of the z-symmetric NCM811 unit cell was set as NCM811 cathode, which is shown in **Supplementary Fig. 3b**. The Buckingham potential parameters representing short-range interactions of NCM811 were taken from the previous study<sup>8</sup>. To calculate the interactions between NCM811 surface and electrolytes, the Buckingham potential parameters<sup>9</sup> were changed into 12-6 Lennard-Jones

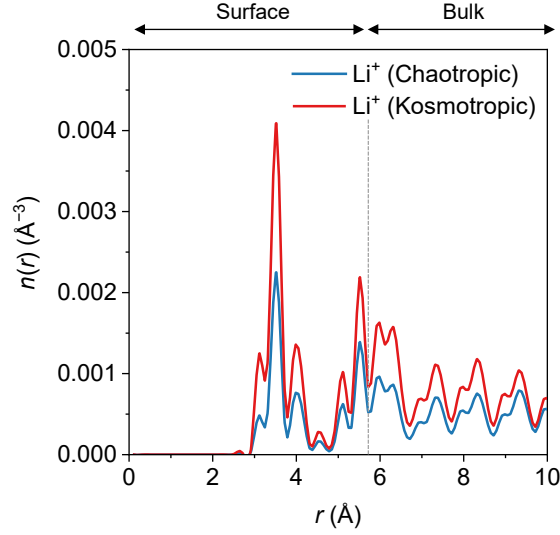
potential parameters. Atomic charge of the NCM811 cathode was calculated by bader charge analysis<sup>10</sup> after DFT calculation. The DFT calculation was performed using Vienna Ab-initio Simulation Package<sup>11</sup> (VASP) 6.2.0 program. The surface of the z-symmetric NCM811 unit cell perpendicular to the z-axis with 10 Å of vacuum layer along the z axis was used. The Perdew–Burke–Ernzerh<sup>12</sup> (PBE) functional was used and the plane-wave basis was cut off by 520 eV. The self-consistent field (SCF) was converged to  $1.0 \times 10^{-6}$  eV and Monkhorst-Pack (M-P) k-point meshes of  $3 \times 3 \times 1$  was used.



**Supplementary Fig. 4 | Simulated structure of electrolytes.** a-c, The snapshots of all components of each electrolyte (a), the aqueous electrolyte system (b), and NCM811 with the aqueous electrolyte systems (c). In the NCM811 with aqueous electrolyte system, the periodic boundary condition (PBC) line above the electrolyte was not displayed because of a thick vacuum layer. The initial and final structure of electrolytes are provided in **Supplementary Data 3-16**.



**Supplementary Fig. 5 | Number density distribution function ( $n(r)$ ) of water in the aqueous solutions at the NCM811 surface.** The surface region was defined as a distance ( $r$ )  $< 5.75 \text{ \AA}$ , where the water forms an electric double layer.



**Supplementary Fig. 6 | Number density distribution function ( $n(r)$ ) of  $\text{Li}^+$  in the aqueous solutions at the NCM811 surface.** The surface region was defined as a distance ( $r$ ) < 5.75 Å, where the water forms an electric double layer.

**Supplementary Note 3 | Calculation of local hydration structure of the aqueous solutions at NCM811 cathode material surface.**

The distribution of  $\text{Li}^+$  did not change significantly according to the anion species, but the  $\text{Li}^+$  concentration at the electrode surface increased in the kosmotropic electrolyte as a consequence of the strong  $\text{Li}^+ \text{-SO}_4^{2-}$  association<sup>13</sup>. This local high concentration of  $\text{Li}^+$  at the surface may contribute to mitigate the  $\text{Li}^+$  leaching<sup>14</sup>.

The residence time correlation function ( $C(t)$ ) was calculated using neighbor function  $H(r_{ij}, t)$  and each function was obtained using equations (2) and (3).

$$(2) \quad H(r_{ij}, t) = \begin{cases} 0, & \text{if } r_{ij} \geq r_{ij}^c \\ 1, & \text{if } r_{ij} < r_{ij}^c \end{cases}$$

$$(3) \quad C(t) = \frac{\sum_{ij}^N \langle H(r_{ij}, t) H(r_{ij}, 0) \rangle}{\sum_{ij}^N \langle H(r_{ij}, 0) H(r_{ij}, 0) \rangle}$$

$r_{ij}$  denotes the pair distance between  $i$  and  $j$ , and  $r_{ij}^c$  denotes the cutoff distance. The cutoff distances between atoms, as well as between the NCM811 cathode surface and water, were determined based on the first coordination shell radius obtained from the radial distribution function and the water density distribution, respectively. The residence time ( $\tau_{\text{water}}$ ) was calculated by integrating the residence time correlation function using equation (4).

$$(4) \quad \tau_{\text{water}} = \int_0^\infty C_i(t) dt$$

Since the reactivity of water interacting with ions decreases<sup>15</sup>, free water on the surface region of the NCM811 cathode was determined to have no hydrogen bonds between the water and ions. The stabilization energy of water molecules ( $\Delta E_i$ ) was determined using the following equations (5) and (6).

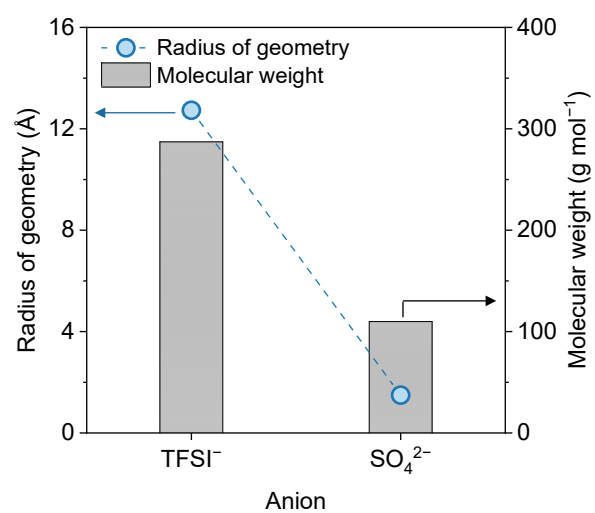
$$(5) \quad E_i = \frac{E_{\text{tot},i} - E_{\text{bulk},i} - E_{\text{cathode}}}{n_{\text{H}_2\text{O},i}}$$

$$(6) \quad \Delta E_i = E_i - E_{\text{H}_2\text{O}}$$

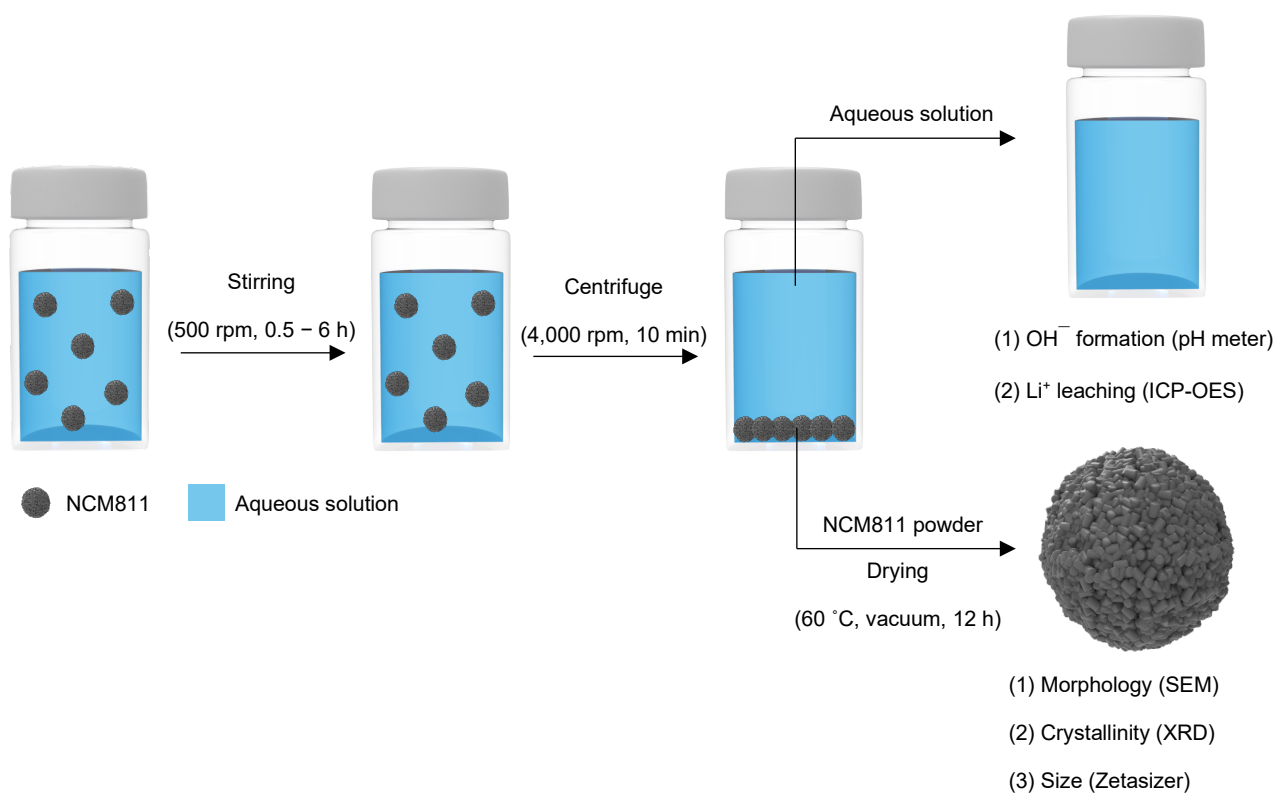
Notation  $i$  denotes the kinds of electrolyte,  $E_i$  denotes the interaction energy between water and

NCM811 cathode,  $E_{\text{tot},i}$  denotes the energy of the total system,  $E_{\text{bulk},i}$  denotes the energy of the surface electrolyte system and  $n_{\text{H}_2\text{O},i}$  denotes the number of water molecules. Since atoms of NCM811 cathode are fixed, predetermined energy ( $E_{\text{cathode}}$ ) value was used.

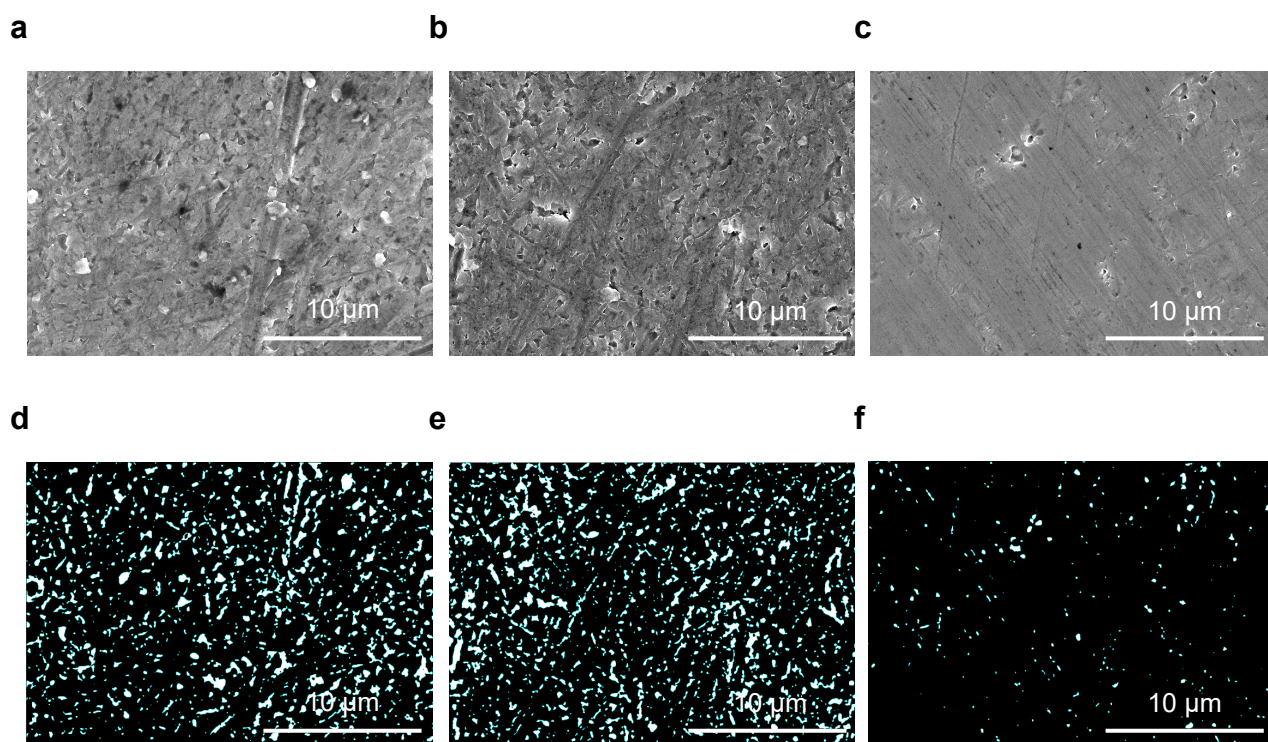




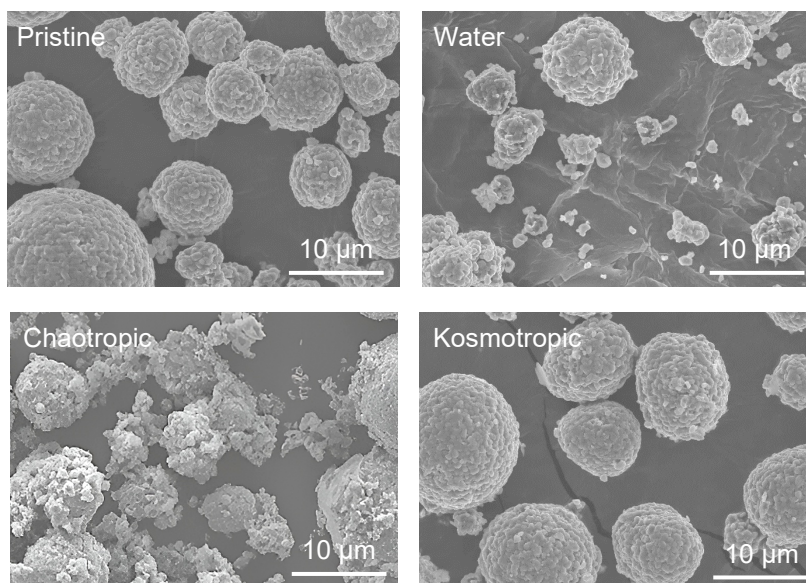
**Supplementary Fig. 7 | Molecular weight and radius of geometry of anions.** (left) TFSI<sup>-</sup> and (right) SO<sub>4</sub><sup>2-</sup>, respectively.



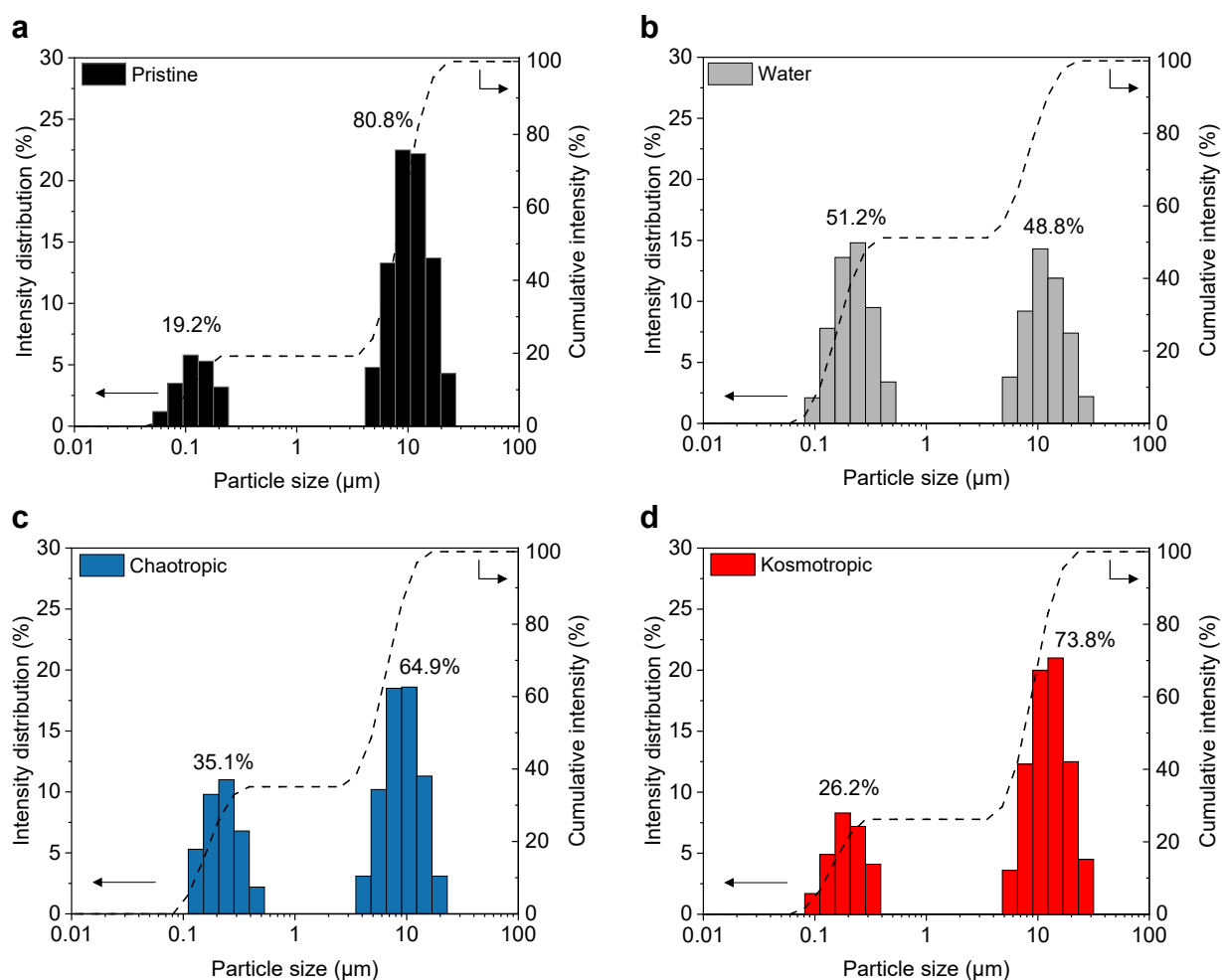
**Supplementary Fig. 8 | Schematic depicting the study model used to investigate the chemical reactivity of the aqueous solutions with cathode materials for aqueous electrode processing.**



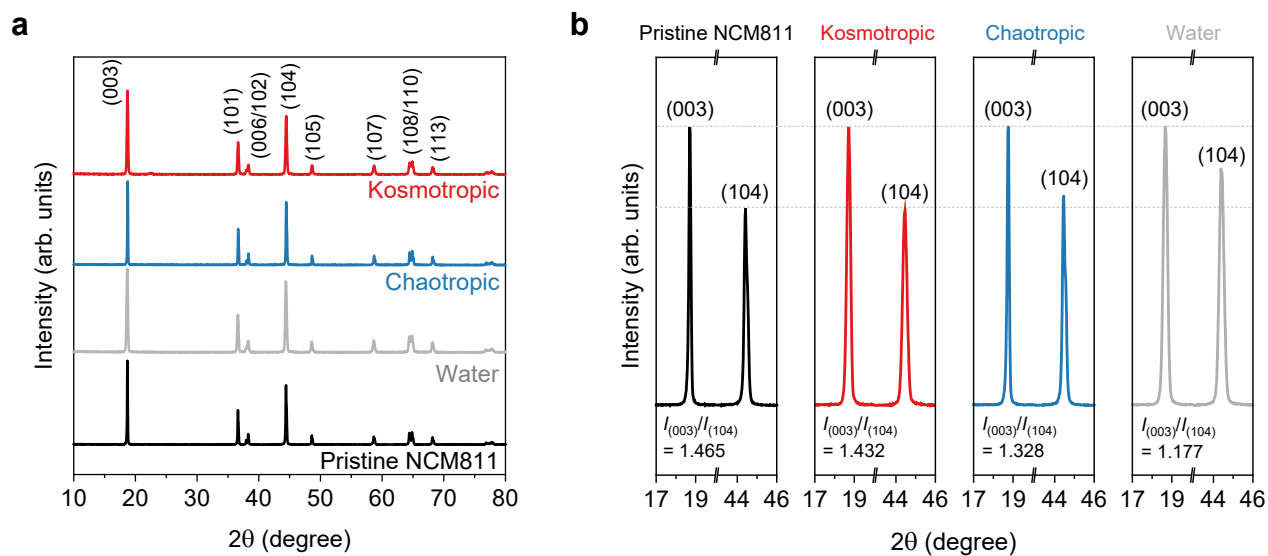
**Supplementary Fig. 9 | Surface image of Al current collectors after aqueous processing.** a-f, Scanning electron microscopy (SEM) images (a-c) and the corresponding binary thresholding images (d-f) of the Al current collectors after the collection of the water-processed (a,d), chaotropic-processed (b,e), and kosmotropic-processed (c,f) NCM811 cathodes. Casted electrodes were removed using ethanol. The binary images were generated by applying 34% of the threshold program to the SEM images, where the areas of corrosion are depicted in white and uncorroded regions are displayed in black.



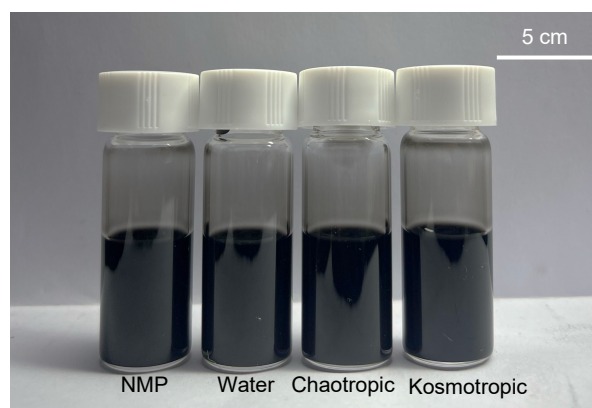
**Supplementary Fig. 10 | Morphology of NCM811 particles after aqueous processing.** SEM images of the pristine NCM811 powders after immersion in water, chaotropic solution and kosmotropic solution for 6 h.



**Supplementary Fig. 11 | Particle size of NCM811 after aqueous processing. a-d,** Particle size distribution of the pristine NCM811 particles (**a**), and NCM811 particles after immersion in various processing solutions (**b-d**): water (**b**), chaotropic solution (**c**), and kosmotropic solution (**d**). The percentages indicate the proportion of primary and secondary particles present in each processing solution.



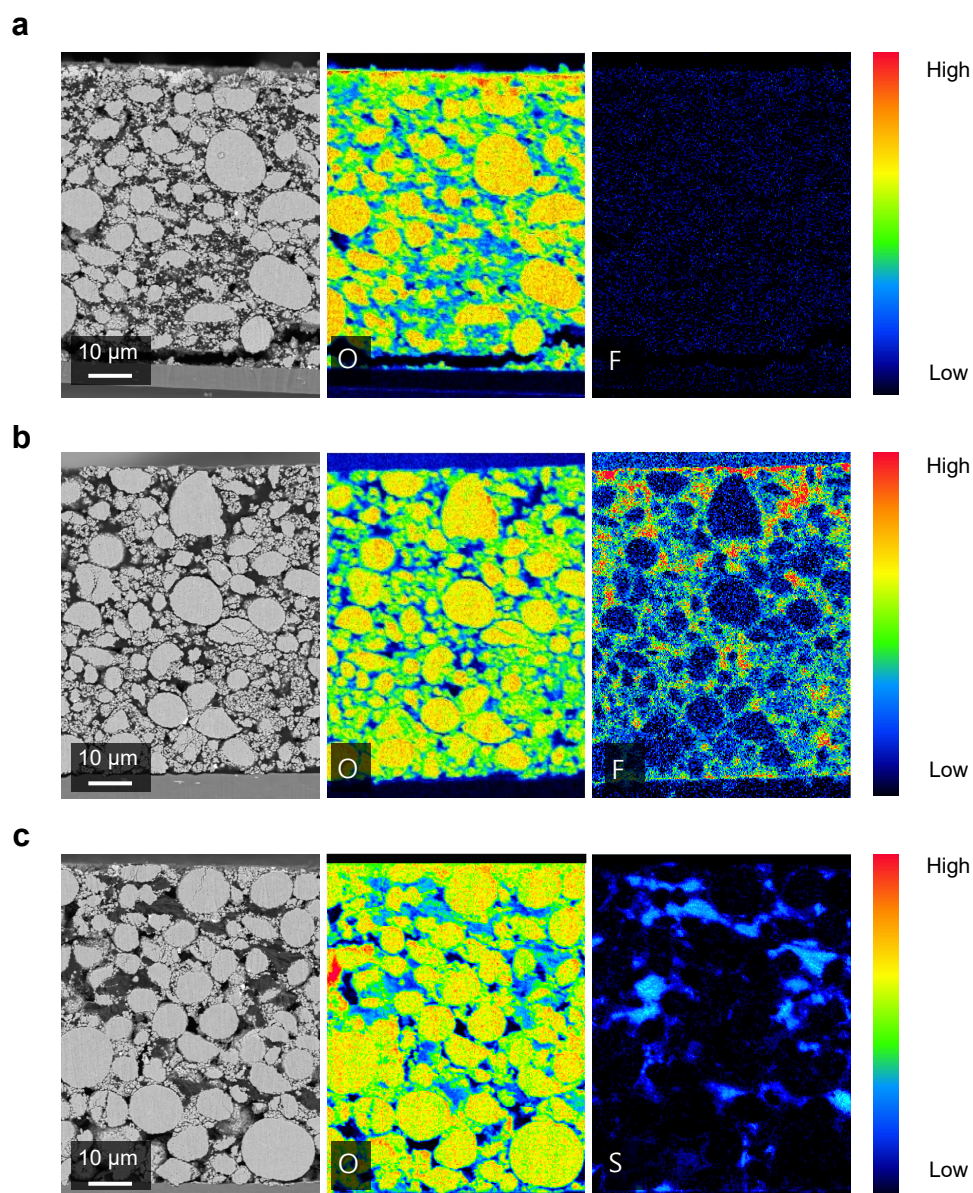
**Supplementary Fig. 12 | Crystal structure of NCM811 after aqueous processing.** **a**, X-ray diffraction (XRD) patterns of NCM811 powders after immersion in water, chaotropic solution, and kosmotropic solution for 6 h. **b**, Magnified XRD patterns, which is normalized by the intensity of (003) peak, highlighting the  $I_{003}/I_{104}$  ratio for the NCM811 powders.



**Supplementary Fig. 13 | Dispersion stability of aqueous solution-processed cathode slurries.**

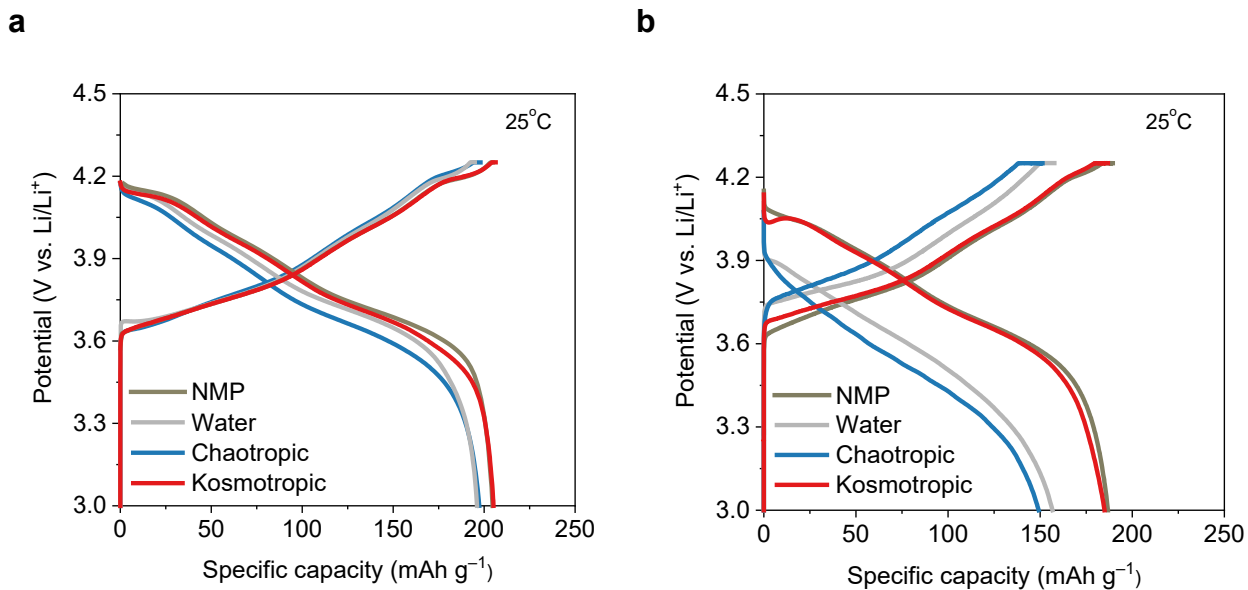
Photographs of the NCM811 electrode slurries prepared using NMP, water, chaotropic solution, and kosmotropic solution, respectively.



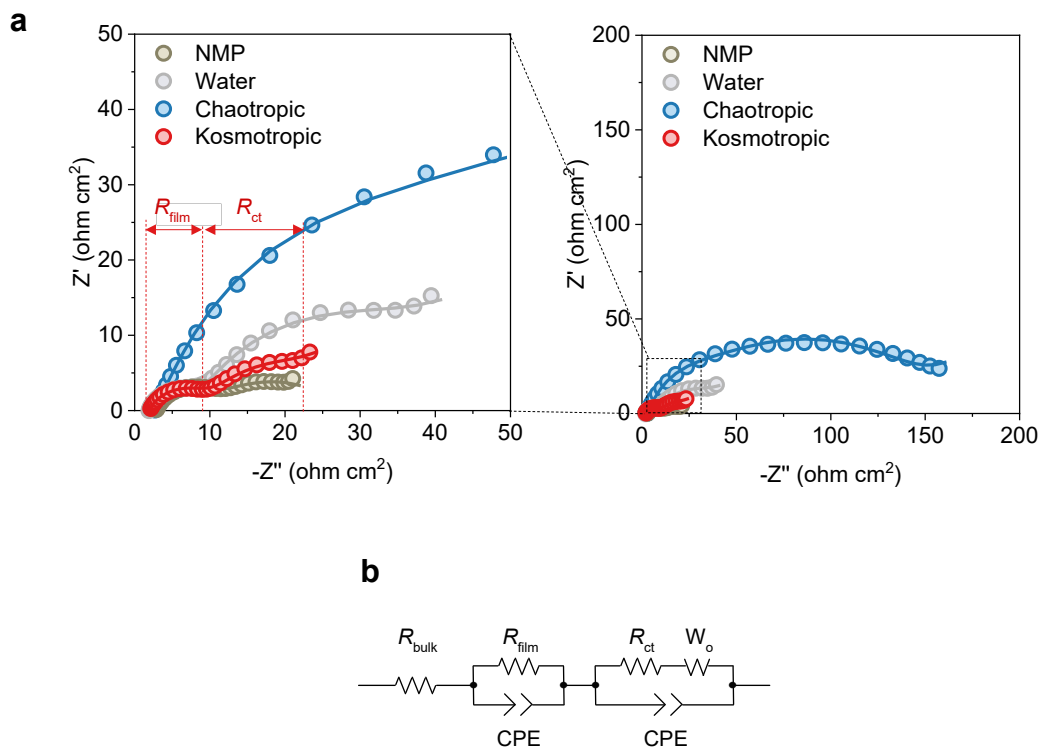


**Supplementary Fig. 14 | Morphology of aqueous solution-processed cathodes.** **a-c**, Cross-sectional scanning electron microscopy (SEM) and electron probe microanalysis (EPMA) elemental mapping (element: O, F, and S) images of the aqueous solution-processed cathodes: water (**a**), chaotropic solution (**b**), kosmotropic solution (**c**). The F and S elements indicate the presence and distribution of the salt additives (LiTFSI was used in the chaotropic solution and  $\text{Li}_2\text{SO}_4$  was used in the kosmotropic solution).

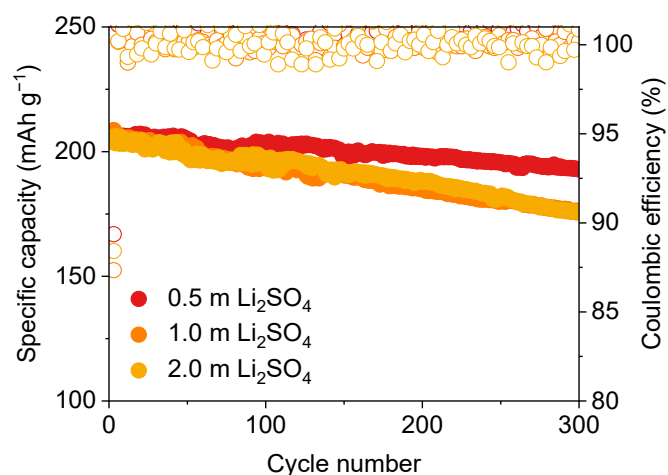




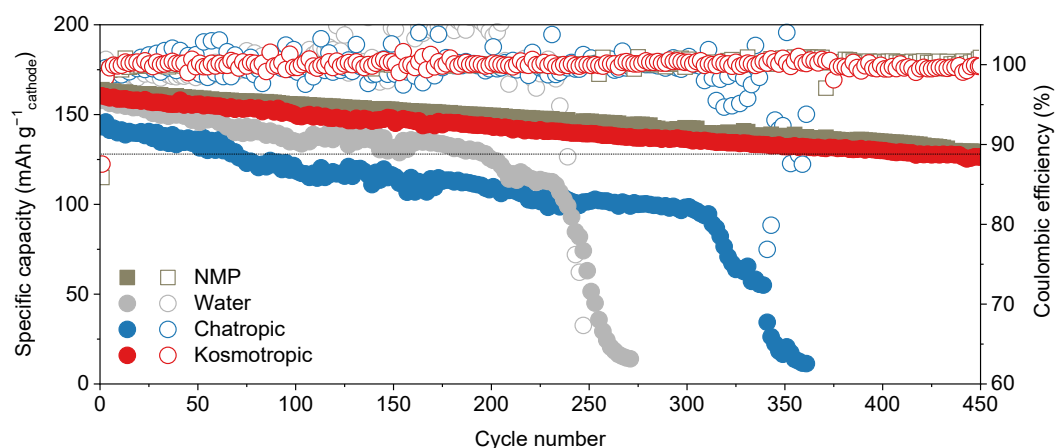
**Supplementary Fig. 15 | Electrochemical performance of cathodes with different processing solutions. a,b,** Galvanostatic charge/discharge profiles of the cathodes at a mass loading of 18.2 mg cm<sup>-2</sup> at a charge/discharge current rate of 0.2 C/0.5 C (1C = 3.74 mA cm<sup>-2</sup>): 1<sup>st</sup> cycle (**a**) and 200<sup>th</sup> cycle (**b**). The electrochemical tests were conducted within a voltage range of 3.00–4.25 V and at a temperature of 25°C.



**Supplementary Fig. 16 | Electrochemical impedance of cathodes with different processing solutions. a**, Nyquist plots of the cycled cathodes at a mass loading of  $18 \text{ mg cm}^{-2}$  after the 400<sup>th</sup> cycle. **b**, The symbols and solid lines represent experimental data and fitted curves, respectively. **b**, Equivalent circuit used to fit the curves.

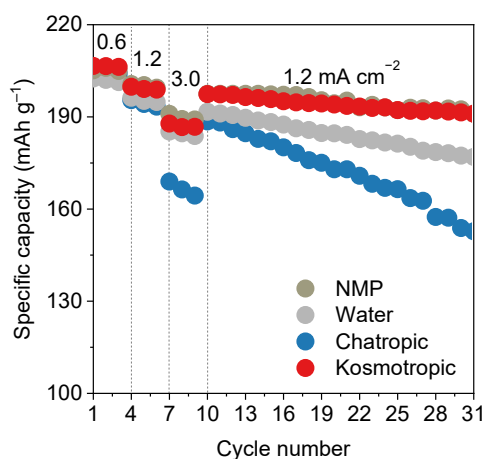


**Supplementary Fig. 17 | Electrochemical cycle performance of cathodes by varying the molality of kosmotropic aqueous processing solution.** Cycle retention of the kosmotropic solution-processed cathodes at a cathode material mass loading of  $18.2 \text{ mg cm}^{-2}$  as a function of the  $\text{Li}_2\text{SO}_4$  concentration of the kosmotropic aqueous processing solution at a current rate of  $0.2 \text{ C}/0.5 \text{ C}$  ( $1\text{C} = 3.74 \text{ mA cm}^{-2}$ ). The slightly poor cycle retention at  $1.0$  and  $2.0 \text{ m Li}_2\text{SO}_4$  may be attributed to the pore blockage of the precipitated salt due to the excessive incorporation. The electrochemical tests were conducted within a voltage range of  $3.00\text{--}4.25 \text{ V}$  and at a temperature of  $25^\circ\text{C}$ .

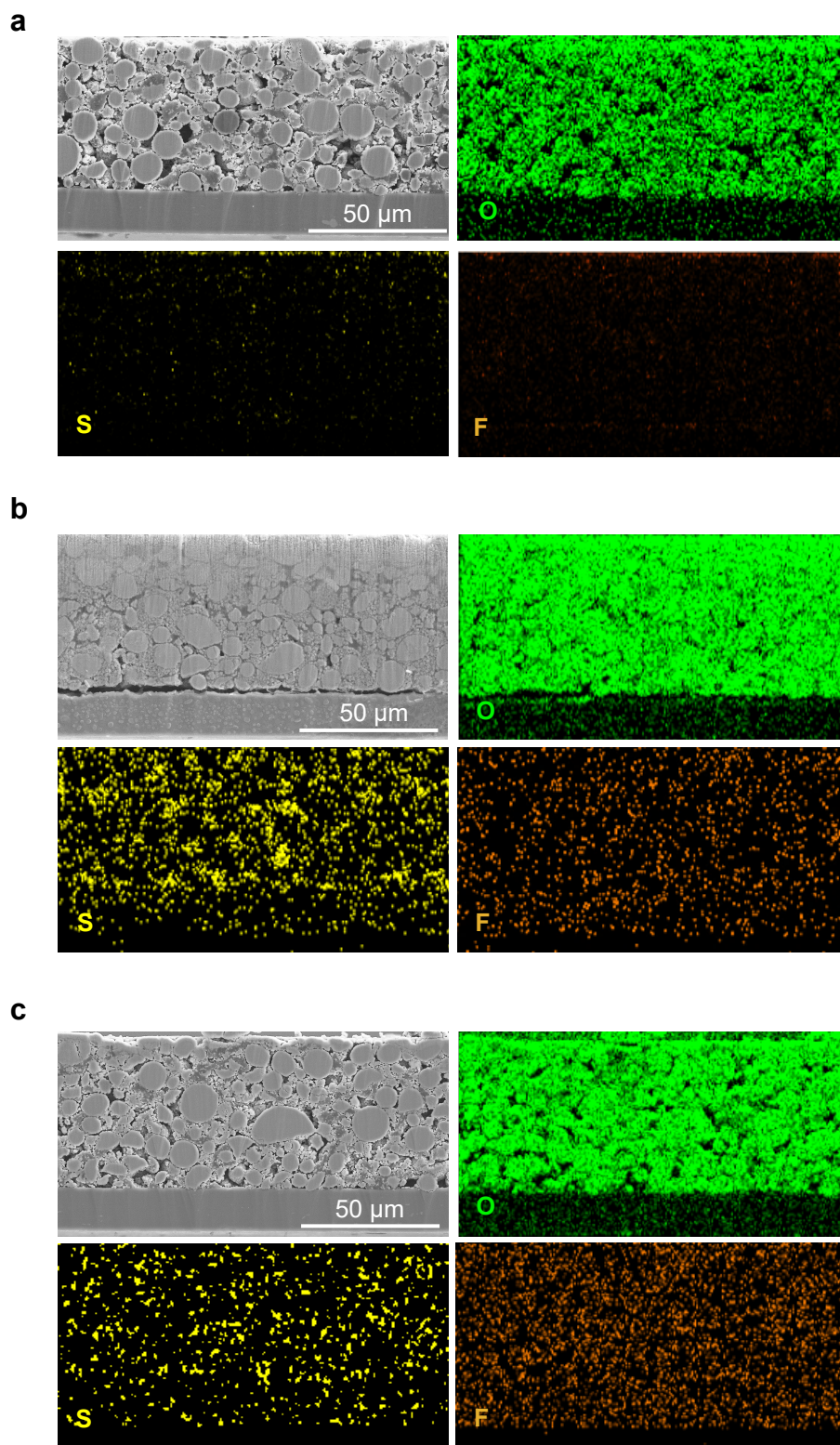


**Supplementary Fig. 18 | Electrochemical cycle performance of cathodes based on cathode mass.**

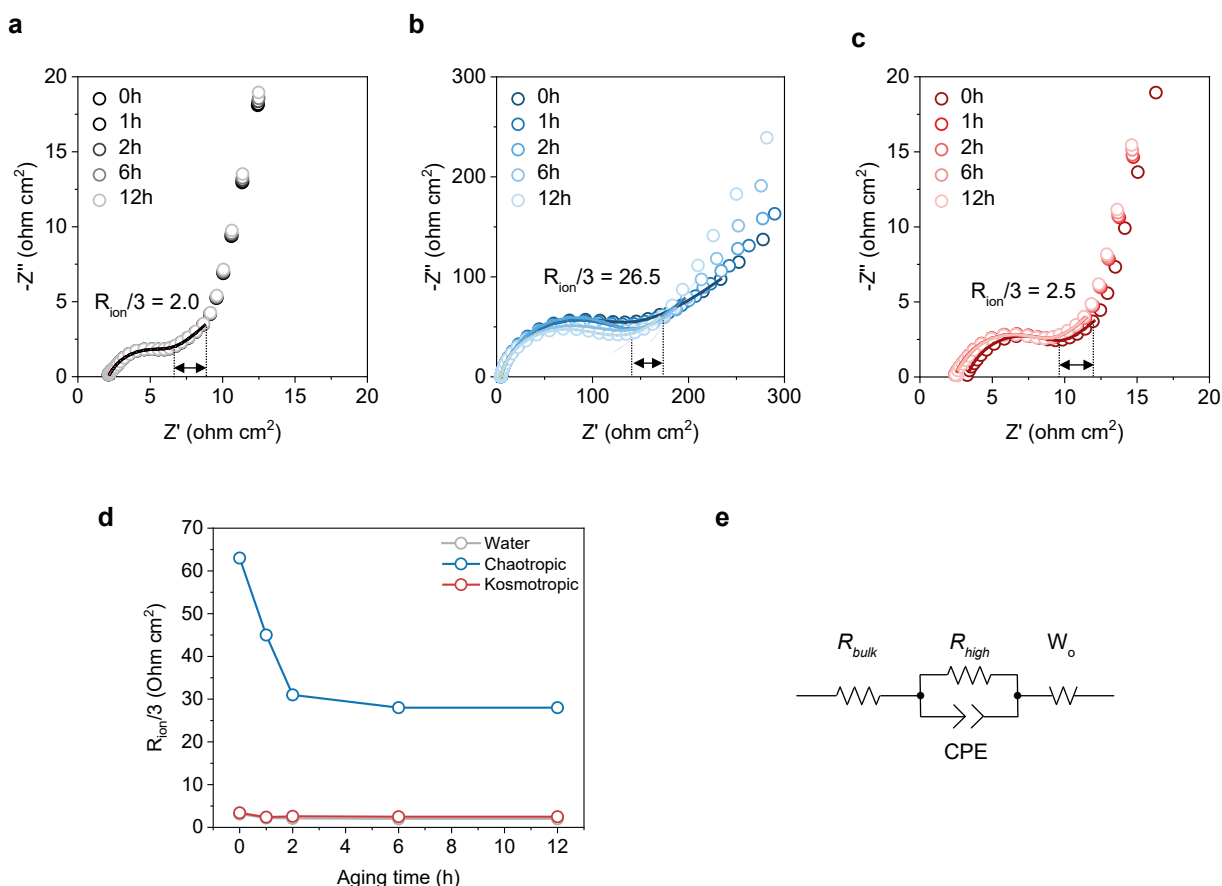
Cycling retention (expressed as discharge specific capacities of cathodes based on their total mass including that of the salt additives) of the cathodes at a current rate of 0.2 C/0.5 C ( $1C = 3.74 \text{ mA cm}^{-2}$ ). The electrochemical tests were conducted within a voltage range of 3.00–4.25 V and at a temperature of 25°C.



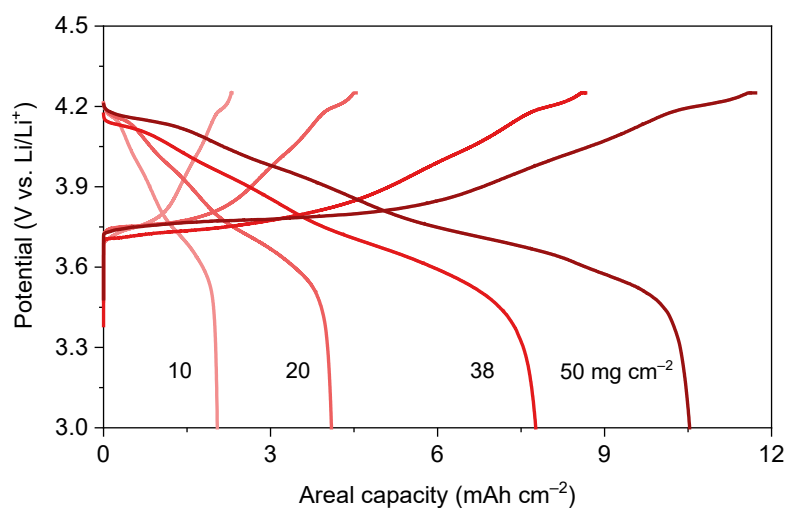
**Supplementary Fig. 19 | Electrochemical rate performance of cathodes with different processing solutions.** Discharge rate capability (discharge current rate = 0.6 mA cm<sup>-2</sup> (for 3 cycles), 1.2 mA cm<sup>-2</sup> (for 3 cycles), and 3.0 mA cm<sup>-2</sup> (for 3 cycles) of the cathodes at an areal capacity of 6 mAh cm<sup>-2</sup> under a fixed charge current density of 1.2 mA cm<sup>-2</sup>. The electrochemical tests were conducted within a voltage range of 3.00–4.25 V and at a temperature of 25°C.



**Supplementary Fig. 20 | Elemental distribution of aqueous solution-processed cathodes. a-c,** Cross-sectional SEM and corresponding EDS images (elements: O, S, F) of the water-processed (a), chaotropic solution-processed (b), and kosmotropic solution-processed (c) NCM811 cathodes.

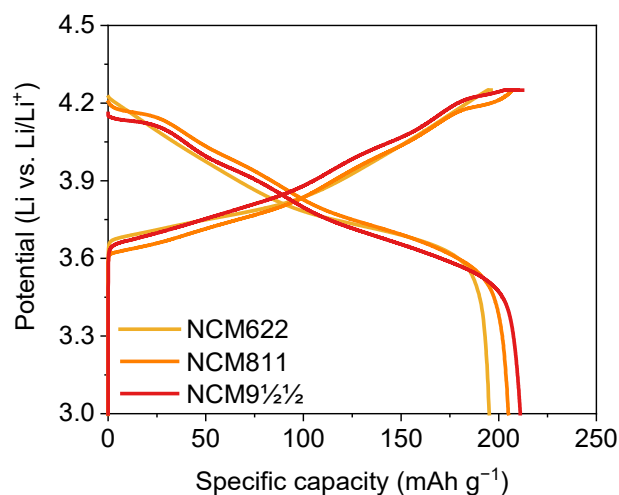


**Supplementary Fig. 21 | Ion transport resistance of aqueous solution-processed cathodes. a-c,** Nyquist plots of the water-processed (**a**), chaotropic solution-processed (**b**), and kosmotropic solution-processed (**c**) cathodes obtained using a symmetric cell configuration (electrode||electrode) as a function of the aging time under a limited amount of liquid electrolytes (electrolyte mass/electrode capacity (E/C) ratio of 2 g Ah<sup>-1</sup> for each electrode). The state of charge (SOC) of each electrode was set to 0% (fully-lithiated state). The symbol and solid lines represent experimental data and fitted curves based on a transmission line equivalent circuit model (TLM), respectively<sup>16</sup>. The projection of a slope to real axis (observed in the low-frequency region of Nyquist plot) reflects the ionic resistance inside the electrodes ( $R_{\text{ion}}$ ) divided by 3. **d**, Change in the  $R_{\text{ion}}$  as a function of the aging time. **e**, Equivalent circuit model based on the generalized finite length Warburg element open circuit terminus ( $Z_w$ ).  $W_o$  was used to estimate  $R_{\text{ion}}$ <sup>17</sup>.

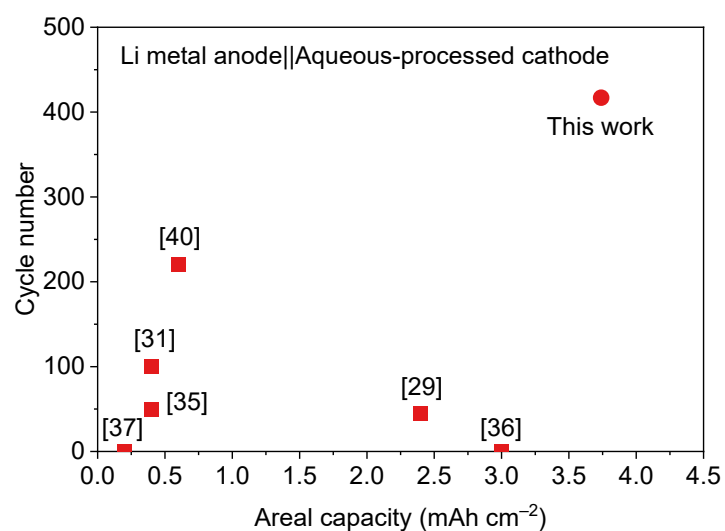


**Supplementary Fig. 22 | Electrochemical performance of kosmotropic aqueous solution-processed cathodes with different mass loadings.** Galvanostatic charge/discharge profiles as a function of mass loading of kosmotropic solution-processed cathodes at a formation cycle. The electrochemical tests were conducted at current rate of 0.1C/0.1C, within a voltage range of 3.00–4.25 V and at a temperature of 25°C.

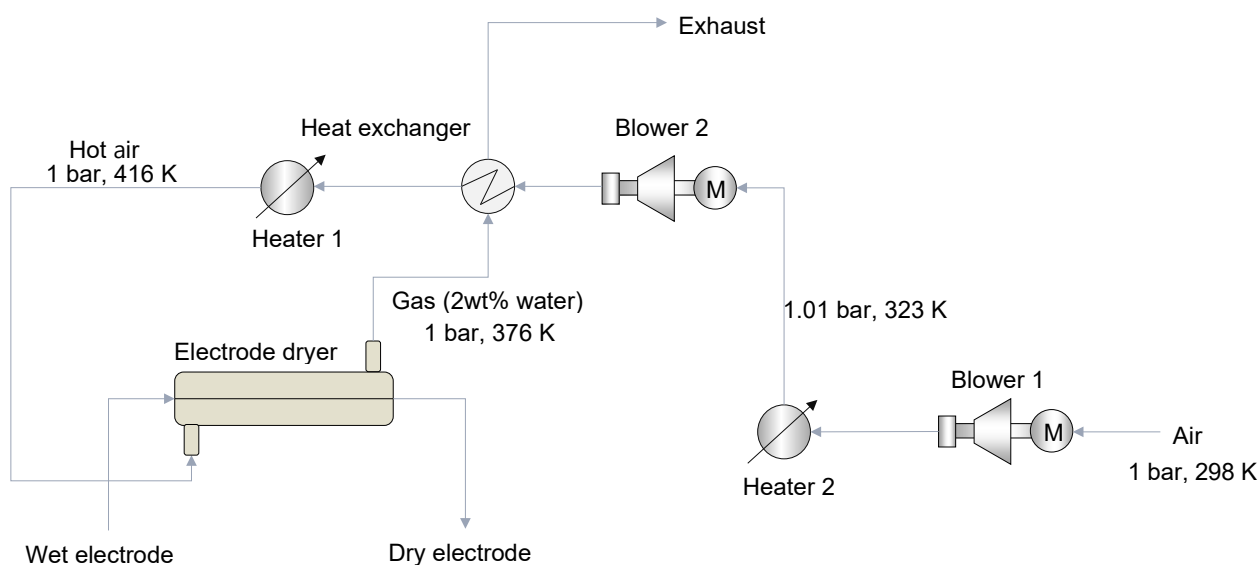




**Supplementary Fig. 23 | Electrochemical performance of kosmotropic aqueous solution-processed cathodes with different active materials.** Galvanostatic charge/discharge profiles of the kosmotropic solution--processed NCM622, NCM811, and NCM9½½ cathodes at a current rate of 0.1 C/0.2 C. The current rate of 1 C =  $x \text{ mA g}^{-1}_{\text{active material}}$  ( $x = 195, 205$ , and  $215$  for NCM622, NCM811, and NCM 9½½ active material, respectively). The cathode material mass loadings were  $18.2 \text{ mg cm}^{-2}$ . The electrochemical tests were conducted within a voltage range of 3.00–4.25 V and at a temperature of 25°C.



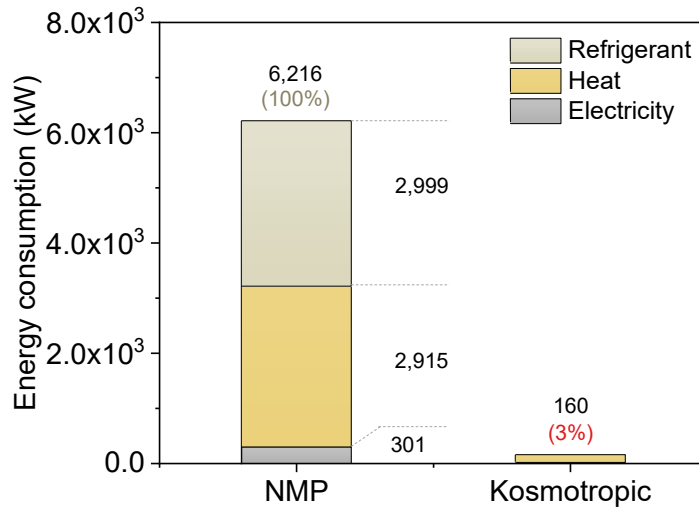
**Supplementary Fig. 24 | Comparison of the kosmotropic aqueous solution-processed cathode (this work) and the previously reported aqueous solution-processed cathodes.** Areal capacity and cycle number of the cathode containing Li-metal batteries were analyzed. The inset numbers correspond to the reference listed in **Supplementary Table 7**.



**Supplementary Fig. 25 | Process flow diagram of the electrode manufacturing based on kosmotropic aqueous processing solution.**

#### **Supplementary Note 4 | Simulation model of cathode manufacturing process.**

The overall unit operation of cathode drying process, including solvent evaporation and recovery, is simulated using corresponding unit modules in the commercial process simulator Aspen Plus V12<sup>18</sup>. To calculate physical properties of solvents, the Non-Random-Two-Liquid (NRTL) method was selected and implemented in the simulator<sup>19</sup> to calculate vapor-liquid and liquid-liquid equilibrium of non-ideal solution. In order to achieve the target solvent evaporation and recovery efficiencies, the specific design and operational parameters for each unit, which are referred from Ahmed, Shabbir, et al<sup>20</sup> are defined and presented in **Supplementary Table 8**.



**Supplementary Fig. 26 | Analysis of the energy consumption of the electrode manufacturing processes (NMP vs. kosmotropic solution).**

**Supplementary Note 5 | Techno-economic analysis of cathode manufacturing process.**

Using the process model with the specified design and operating parameters, the levelized cost of cathode drying (*LCOD*) is calculated for both the NMP and aqueous solution-based manufacturing system based on equation (7).

$$(7) \quad LCOD = \frac{CAPEX \times \frac{r(1+r)^n}{(1+r)^n - 1} + OPEX}{m_{\text{cathode}}}$$

where *CAPEX* is the capital expenditure of the cost functions,  $\frac{r(1+r)^n}{(1+r)^n - 1}$  is the capital recovery factor with plant life year *n* and interest rate *r*, *OPEX* is the annual operating expenditure.

## Estimation of *CAPEX*

The *CAPEX* is determined using the bare module cost approach<sup>21</sup>, which considers the construction cost of the plant, encompassing equipment purchase costs and both direct and indirect costs associated with the installation of each unit. Bare module cost calculation was conducted using equipment type, capacity, and operating condition specified in process model. The detailed calculation procedure is presented as follows.

Firstly, the purchase cost of unit equipment is calculated using equations (8).

$$(8) \quad \log_{10} C_p^o = K_1 + K_2 \log_{10} A + K_3 \log_{10} A^2$$

where  $C_p^o$  and  $A$  represent the purchase cost and capacity of the equipment, respectively.

The coefficients of the equations with equipment types, capacity units, and applicable ranges of the purchase costs are listed in **Supplementary Table 9**.

The specified operating conditions of the unit result in a difference in costs from the reference purchase cost. The bare module approach accounts for this cost variation by considering factors such as operating pressure and material properties. In addition, the installation of purchased equipment incurs additional direct and indirect costs, including labor, freight, overheads, and engineering factors. In summary, the capital cost, which includes both the purchase and installation costs, can be calculated based on equation (9).

$$(9) \quad C_{BM} = C_p^o (B_1 + B_2 F_M F_p)$$

where  $B_1$  and  $B_2$  are the bare module factors, of which detail values and calculation method are described in Turton, Richard, et al<sup>21</sup>.

When constructing desired manufacturing system, additional costs can be categorized into two groups: contingency and fee costs, and auxiliary facilities costs. In the absence of specific information, it was assumed that contingency costs would amount to 15% of the equipment cost, while fee costs would be 3% of the equipment cost<sup>21</sup>. On the other hand, auxiliary facility costs are primarily influenced by site development, auxiliary buildings, and utilities, rather than the operating pressure or construction materials for the equipment. Due to the absence of corresponding data, for the base case condition, these costs were conservatively estimated to be 50% of the equipment cost<sup>21</sup>.

$$(10) \quad CAPEX = 1.18 \sum_{i=1}^n C_{BM,i} + 0.50 \sum_{i=1}^n C_{BM,i}^o$$

where  $C_{BM,i}$  is the equipment cost, and  $C_{BM,i}^o$  is the equipment cost for the base case's condition.

### Estimation of *OPEX*

*OPEX* is a summation of the annual operating costs computed as following equation (11).

$$(11) \quad OPEX = C_{\text{main}} + C_{\text{ele}} + C_{\text{cool}} + C_{\text{heat}} + C_{\text{water}} + C_{\text{labor}} \times N_{\text{OL}}$$

where  $C_{\text{main}}$  is the maintenance cost,  $C_{\text{ele}}$  is the grid electricity cost,  $C_{\text{cool}}$  is the cooling cost,  $C_{\text{heat}}$  is the heat utility cost,  $C_{\text{water}}$  is the process water cost,  $C_{\text{labor}}$  is the annual salary per operator, and  $N_{\text{OL}}$  is the operating labor for the overall system which is suggested in **Supplementary Table 10**.

The operating labor  $N_{\text{OL}}$  for the chemical plant was estimated as follows<sup>21</sup>

$$(12) \quad N_{\text{OL}} = 4.5(6.29 + 31.7N_{\text{p}} + 0.23N_{\text{np}})^{0.5}$$

where  $N_{\text{p}}$  is the processing steps of handling particles, and  $N_{\text{np}}$  is the nonparticulate steps, including gas compression, fluid reactor, and heat exchangers.

## Supplementary Tables

**Supplementary Table 1** | Nonbonded parameters for NCM811. Atomic partial charges were calculated in this work.

| Atom | $q(e)$ | $\sigma$<br>[nm]       | $\varepsilon$<br>[kJ mol <sup>-1</sup> ] |
|------|--------|------------------------|--|
| Li   | +0.86  | $5.539 \times 10^{-1}$ | $1.479 \times 10^{-3}$                   |
| Ni   | +1.00  | $5.606 \times 10^{-1}$ | $6.057 \times 10^{-3}$                   |
| Co   | +1.26  | $6.003 \times 10^{-1}$ | $6.545 \times 10^{-3}$                   |
| Mn   | +1.50  | $6.321 \times 10^{-1}$ | $7.230 \times 10^{-3}$                   |
| O    | -0.89  | $1.910 \times 10^{-1}$ | 1.918                                    |



**Supplementary Table 2** | **a**, Composition of the electrode slurries containing 100 g of electrode components (cathode materials, binder, and conductive additive). **b**, Composition ratio of the aqueous-processed electrodes including that of the salt additives.

**a**

| Processing solution   | Cathode material<br>[g] | Binder<br>[g] | Conductive additive<br>[g] | Salt additive<br>[g] |
|---|-------------------------|---------------|----------------------------|----------------------|
| NMP   | 95.5                    | 2.5           | 2.0                        | -                    |
| H <sub>2</sub> O  | 95.5                    | 2.5           | 2.0                        | -                    |
| Chaotropic solution<br>(1.0 m LiTFSI in H <sub>2</sub> O)                           | 95.5                    | 2.5           | 2.0                        | 11.5                 |
| Kosmotropic solution<br>(0.5 m Li <sub>2</sub> SO <sub>4</sub> in H <sub>2</sub> O) | 95.5                    | 2.5           | 2.0                        | 2.6                  |

**b**

| Processing solution   | Composition<br>[wt.%] |                              |               |
|---|-----------------------|------------------------------|---------------|
|   | Cathode material      | Binder & conductive additive | Salt additive |
| NMP   | 95.5                  | 4.5                          | -             |
| H <sub>2</sub> O  | 95.5                  | 4.5                          | -             |
| Chaotropic solution<br>(1.0 m LiTFSI in H <sub>2</sub> O)                           | 85.9                  | 4.0                          | 10.1          |
| Kosmotropic solution<br>(0.5 m Li <sub>2</sub> SO <sub>4</sub> in H <sub>2</sub> O) | 93.1                  | 4.4                          | 2.5           |

**Supplementary Table 3 | a,b,** Cost information of materials (**a**) and processing solvents (or solutions) (**b**). Cost of the aqueous processing solutions was determined at an equimolar  $\text{Li}^+$  concentration of 1.0 m in  $\text{H}_2\text{O}$ . The material cost information was obtained from their suppliers.

**a**

| Component | Material                        | Weight [g] | Cost [USD] | Specific cost [USD g <sup>-1</sup> ] |
|-----------|---------------------------------|------------|------------|--------------------------------------|
| Solvent   | H <sub>2</sub> O                | 10,000     | 499.1      | 0.01                                 |
|           | NMP                             | 515        | 255.0      | 0.50                                 |
| Salt      | LiTFSI                          | 100        | 552.0      | 5.52                                 |
|           | LiOTf                           | 100        | 401.2      | 4.01                                 |
|           | LiOAc                           | 500        | 389.5      | 0.78                                 |
|           | Li <sub>2</sub> SO <sub>4</sub> | 500        | 163.0      | 0.33                                 |

**b**

| Processing solution  | Cost [USD g <sup>-1</sup> ] | Cost normalized by NMP |
|--|-----------------------------|------------------------|
| NMP  | 0.5                         | 100%                   |
| H <sub>2</sub> O   | 0.005                       | 1%                     |
| Chaotropic solution (1.0 m LiTFSI in H <sub>2</sub> O)                           | 1.24                        | 249%                   |
| 1.0 m LiOTf in H <sub>2</sub> O  | 0.55                        | 110%                   |
| 1.0 m LiOAc in H <sub>2</sub> O  | 0.05                        | 11%                    |
| Kosmotropic solution (0.5 m Li <sub>2</sub> SO <sub>4</sub> in H <sub>2</sub> O) | 0.02                        | 4%                     |

**Supplementary Table 4 | a**, Cost information of the cathode components. Material specifications are described in Methods. **b**, Calculation details of the specific capacity based on the material cost of cathodes and processing solutions, which are normalized by electrode area of 1 cm<sup>2</sup>. The solid content of the electrode slurries was 53 wt.%. The material cost information was obtained from their suppliers.

**a**

| Component           | Material     | Weight [g] | Cost [USD] | Specific cost [USD g <sup>-1</sup> ] |
|---------------------|--------------|------------|------------|--------------------------------------|
| Cathode material    | NCM811       | 500        | 345        | 0.69                                 |
| Binder              | PAA          | 250        | 407        | 1.63                                 |
|                     | CMC          | 1,000      | 168        | 0.17                                 |
|                     | PVdF         | 100        | 120        | 1.20                                 |
| Conductive additive | Carbon black | 400        | 214        | 0.54                                 |

| Component         | Material | Area [m <sup>2</sup> ] | Cost [USD] | Areal cost [USD m <sup>-2</sup> ] |
|-------------------|----------|------------------------|------------|-----------------------------------|
| Current collector | Al       | 98                     | 295        | 3.01                              |

**b**

| Electrodes (prepared using the following solution)                               | Areal capacity [mAh cm <sup>-2</sup> ] | Cathode cost [USD] | Solution cost [USD] | Capacity normalized by material cost [mAh USD <sup>-1</sup> ] |
|--|--|--------------------|---------------------|---|
| NMP  | 3.74                                   | 0.01367            | 0.00847             | 169   |
| H <sub>2</sub> O   | 3.61                                   | 0.01352            | 0.00008             | 265   |
| Chaotropic solution (1.0 m LiTFSI in H <sub>2</sub> O)                           | 3.59                                   | 0.01352            | 0.02101             | 104   |
| Kosmotropic solution (0.5 m Li <sub>2</sub> SO <sub>4</sub> in H <sub>2</sub> O) | 3.74                                   | 0.01352            | 0.00034             | 270   |

**Supplementary Table 5 | a**, Molar mass of the LiTFSI and Li<sub>2</sub>SO<sub>4</sub> salts. **b**, Calculation details of the specific capacity based on the total mass including that of the salt additives. The masses of the cathode material, binder, conductive additive, and Al current collector were 18.2, 0.5, 0.4, and 4.0 mg cm<sup>-2</sup>, respectively.

**a**

| Li salt additive                | Density [g mL <sup>-1</sup> ] | Molar mass [g mol <sup>-1</sup> ] | Mass [g mol <sub>Li</sub> <sup>-1</sup> ] | Molar volume [mL mol <sup>-1</sup> ] | Volume [mL mol <sub>Li</sub> <sup>-1</sup> ] |
|---------------------------------|-------------------------------|-----------------------------------|---|--------------------------------------|--|
| LiTFSI                          | 1.3                           | 287.1                             | 287.1                                     | 215.8                                | 215.8  |
| Li <sub>2</sub> SO <sub>4</sub> | 2.2                           | 109.9                             | 55.0                                      | 49.5                                 | 24.8   |

**b**

| Processing solution   | Areal capacity [mAh cm <sup>-2</sup> ] | Residual salt [mg cm <sup>-2</sup> ] | Areal mass [mg cm <sup>-2</sup> ] | Specific capacity [mAh g <sub>cathode</sub> <sup>-1</sup> ] |
|---|--|--------------------------------------|-----------------------------------|---|
| NMP   | 3.74                                   | 0                                    | 23.1                              | 162   |
| H <sub>2</sub> O  | 3.61                                   | 0                                    | 23.1                              | 156   |
| Chaotropic solution<br>(1.0 m LiTFSI in H <sub>2</sub> O)                           | 3.59                                   | 2.2                                  | 25.3                              | 142   |
| Kosmotropic solution<br>(0.5 m Li <sub>2</sub> SO <sub>4</sub> in H <sub>2</sub> O) | 3.74                                   | 0.5                                  | 23.6                              | 159   |

**Supplementary Table 6** | Calculation details on the pore volume of the electrode (a), and separator (b) used in this study.

**a**

| Electrode           | Material | Composition<br>[%] | Mass<br>[mg, 12 pi] | True density<br>[g cc <sup>-1</sup> ] | Volume<br>[cc, 12 pi] | Volume<br>[μL, 12 pi] |
|---------------------|----------|--------------------|---------------------|---------------------------------------|-----------------------|-----------------------|
| Active material     | NCM811   | 95.5               | 20.63               | 4.3                                   | 0.0048                | 4.8                   |
| Conductive additive | Super P  | 2                  | 0.43                | 1.6                                   | 0.00027               | 0.27                  |
| Binder              | CMC      | 1.25               | 0.27                | 1.6                                   | 0.00017               | 0.17                  |
|                     | PAA      | 1.25               | 0.27                | 1.15                                  | 0.00023               | 0.23                  |
| Pore                |          |                    |                     |                                       | 0.0017                | 1.7                   |
| Sum                 |          |                    | 21.58               |                                       | 0.0071                |                       |
| Electrode density   |          |                    | 3.00                |                                       |                       |                       |

**b**

| Separator    | Porosity<br>[%] | thickness<br>[μm] | Volume<br>[cc, 18pi] | Volume<br>[μL, 18 pi] |
|--------------|-----------------|-------------------|----------------------|-----------------------|
| Polyethylene | 47              | 16                | 0.0041               |                       |
| Pore         |                 |                   | 0.0019               | 1.91                  |

**Supplementary Table 7** | Comparison of the kosmotropic solution-processed cathodes and previously reported aqueous solution-processed cathodes.

| No.       | Processing solution                                      | Cathode material | Binder               | Specific capacity [mAh g <sup>-1</sup> ] | Areal capacity [mAh cm <sup>-2</sup> ] | AM composition [wt. %] | Ref.      |
|-----------|--|------------------|----------------------|--|--|------------------------|-----------|
| This work | 0.5 m Li <sub>2</sub> O <sub>4</sub> in H <sub>2</sub> O | NCM9½½           | CMC/PAA              | 215                                      | 3.9                                    | 93.1                   | This work |
|           |  | NCM811           | CMC/PAA              | 205                                      | 3.7, 7.8, 10.2                         |                        |           |
|           |  | NCM622           | CMC/PAA              | 195                                      | 3.6                                    |                        |           |
| 1         | H <sub>2</sub> O   | NCM811           | CMC/Acrylic emulsion | 205                                      | 2.3                                    | 90                     | 22        |
| 2         | H <sub>2</sub> O   | NCM811           | Carrageenan          | 200                                      | 2.2                                    | 90                     | 23        |
| 3         | H <sub>2</sub> O   | NCM811           | PDADMA-DEP (or DBP)  | 200                                      | 2.1                                    | 90                     | 24        |
| 4         | H <sub>2</sub> O   | NCM811           | SBR/CMC              | 196                                      | 2.6                                    | 94                     | 25        |
| 5         | Li <sub>2</sub> SO <sub>4</sub> in H <sub>2</sub> O      | NCM811           | CMC                  | 190                                      | 2.4                                    | 92                     | 26        |
| 6         | H <sub>2</sub> O   | NCM811           | CMC/PAA              | 185                                      | 2.6                                    | 93                     | 27        |
| 7         | H <sub>2</sub> O   | NCM811           | CMC/ICN              | 182                                      | 2.6                                    | 93                     | 28        |
| 8         | H <sub>2</sub> O   | NCM811           |                      | 189                                      | 2.6                                    | 90                     | 29        |
|           |  | NCM622           | CMC                  | 169                                      | 2.4                                    | 90                     |           |
|           |  | NCM111           |                      | 153                                      | 2.1                                    | 90                     |           |
| 9         | LiOH in H <sub>2</sub> O                                 | NCM523           | CMC/PAA/PEO          | 158                                      | 2                                      | 91                     | 30        |
| 10        | H <sub>2</sub> O   | NCM424           | CMC                  | 160                                      | 0.4                                    | 80                     | 31        |
| 11        | H <sub>2</sub> O   | NCM111           | CMC                  | 150                                      | 1.1                                    | 88                     | 32        |

|    |  |        |             |     |     |    |    |
|----|--|--------|-------------|-----|-----|----|----|
| 12 | H <sub>3</sub> PO <sub>4</sub> in H <sub>2</sub> O | NCM111 | CMC         | 150 | 1.3 | 88 | 33 |
| 13 | H <sub>2</sub> O                                   | NCA    | CMC         | 182 | 2   | 92 | 34 |
| 14 | H <sub>2</sub> O                                   | LFP    | Xanthan gum | 167 | 0.4 | 87 | 35 |
| 15 | H <sub>2</sub> O                                   | LFP    | NBR/CMC     | 155 | 3   | 90 | 36 |
| 16 | H <sub>2</sub> O                                   | LFP    | PAA         | 150 | 0.2 | 83 | 37 |
| 17 | H <sub>2</sub> O                                   | LFP    | CMC         | 140 | 0.2 | 85 | 38 |
| 18 | H <sub>2</sub> O                                   | LFP    | PEO         | 136 | 0.4 | 73 | 39 |
| 19 | LiTFSI in H <sub>2</sub> O                         | LNMO   | CMC/SBR     | 125 | 2   | 71 | 14 |
| 20 | H <sub>2</sub> O                                   | LMO    | Alginate    | 122 | 0.6 | 75 | 40 |

---

**Supplementary Table 8** | Internal column specifications of the cathode manufacturing process.

| Unit                | Design and operating specification  |
|---------------------|---|
| Blower              | Isentropic efficiency: 0.72   |
| Heater              | Operating pressure: 1 bar<br>Operating temperature: 143°C   |
| Heat exchanger      | Type: Shell and tube type<br>Minimum temperature value: 1°C   |
| Distillation column | Number of stages: 14<br>Types of packed: Mellapak Packed 250Y<br>Column height and diameter: 6 m and 0.2 m<br>Condenser pressure: 1 bar<br>Distillate rate: 2.14 mol/sec<br>Reflux ratio: 0.2 |
| Scrubber            | Number of stages: 3<br>Types of packed: Sieve<br>Column height and diameter: 0.61 m and 1.4 m<br>Top pressure: 1 bar  |
| Dryer               | Type: Convective dryer<br>Length: 40 m<br>Gas flow direction: Counter-current<br>Cathode residence time: 0.5 h  |



**Supplementary Table 9** | Parameters for the estimation of the purchase costs<sup>21</sup>.

| <b>Equipment</b>    | <b>Description</b> | <b><math>K_1</math></b> | <b><math>K_2</math></b> | <b><math>K_3</math></b> | <b>Capacity<br/>[units]</b>                    | <b>Applicable<br/>range</b> |
|---------------------|--------------------|-------------------------|-------------------------|-------------------------|--|-----------------------------|
| Distillation column | Tray and packed    | 3.4974                  | 0.4485                  | 0.1074                  | Volume [m <sup>3</sup> ]                       | 0.3~520                     |
| Scrubber            | Sieve              | 2.9949                  | 0.4465                  | 0.3961                  | Area [m <sup>2</sup> ]                         | 0.07~12.30                  |
| Blower              | Axial tube         | 3.0414                  | -0.3375                 | 0.4722                  | Gas flowrate [m <sup>3</sup> s <sup>-1</sup> ] | 1~100                       |
| Process vessel      | Horizontal         | 3.5565                  | 0.3776                  | 0.0905                  | Volume [m <sup>3</sup> ]                       | 0.1~628                     |
| Cooler              | Flat plate         | 4.6656                  | -0.1557                 | 0.1547                  | Heat transfer surface [m <sup>2</sup> ]        | 10~1,000                    |
| Heater              | Hot water heat     | 2.0829                  | 0.9074                  | -0.0243                 | Heat duty [kw]                                 | 650~10,750                  |
| Heat exchanger      | Fixed tube         | 4.3247                  | -0.3030                 | 0.1634                  | Area [m <sup>2</sup> ]                         | 10~1,000                    |
| Dryer               | Tray               | 3.6951                  | 0.5442                  | -0.1248                 | Area [m <sup>2</sup> ]                         | 1.8~20                      |

**Supplementary Table 10** | Input parameters for the levelized cost of recycling calculation.

| Type                                | Value or range                             |
|-------------------------------------|--|
| Plant life                          | 25 years                                   |
| Annual operating hours of reforming | 8500 h year <sup>-1</sup>                  |
| Discount rate                       | 7.0%                                       |
| Maintenance cost                    | 2.75% of CAPEX                             |
| Grid electricity tariff             | 0.0775 USD kWh <sup>-1</sup>               |
| Heating utility                     | $1.8 \times 10^{-8}$ USD cal <sup>-1</sup> |
| Cooling utility                     | $1.1 \times 10^{-8}$ USD cal <sup>-1</sup> |
| Process water price                 | $6.7 \times 10^{-5}$ USD kg <sup>-1</sup>  |
| Annual salary per operator          | 52,900 \$ year <sup>-1</sup>               |

**Supplementary Table 11** | Comparison of the materials hazards of the kosmotropic aqueous solution (0.5 m Li<sub>2</sub>SO<sub>4</sub> in H<sub>2</sub>O) and NMP by National Fire Protection Association (NFPA 704). The sum of ‘Fire hazards’ and ‘Reactivity’ was used in **Fig. 6e** as a criterion of material safety.

| Electrode processing | Material                        | Fire hazards | Reactivity | Health hazards |
|----------------------|---------------------------------|--------------|------------|----------------|
| Non-aqueous          | NMP                             | 2            | 1          | 2              |
| Aqueous              | H <sub>2</sub> O                | 0            | 0          | 0              |
|                      | Li <sub>2</sub> SO <sub>4</sub> | 0            | 0          | 2              |

**Supplementary Table 12 | a**, Green score of solvents of the kosmotropic aqueous processing solution (0.5 m Li<sub>2</sub>SO<sub>4</sub> in H<sub>2</sub>O) and NMP referred from GlaxoSmithKline (GSK) solvent selection guideline<sup>1,41</sup>. Legislative controls are indicated in the form of a ‘Flag’. **b**, Green score of binders for the kosmotropic aqueous processing solution and NMP<sup>42</sup>.

**a**

| Electrode processing | Solvent          | Waste | Environmental impact | Health | Life cycle assessment | Flag | Green score <sup>†</sup> (0~40) |
|----------------------|------------------|-------|----------------------|--------|-----------------------|------|---------------------------------|
| Non-aqueous          | NMP              | 5     | 6                    | 3      | 4                     | *    | 18                              |
| Aqueous              | H <sub>2</sub> O | 10    | 10                   | 10     | 10                    | -    | 40                              |

**b**

| Electrode processing | Binder | F-free | Processability | Synthesis | Sustainability | Ease of disposal | Green score <sup>††</sup> (-5~+5) |
|----------------------|--------|--------|----------------|-----------|----------------|------------------|-----------------------------------|
| Non-aqueous          | PVdF   | —      | —              | —         | —              | —                | -5                                |
| Aqueous              | CMC    | +      | +              | +         | +              | +                | +5                                |
|                      | PAA    | +      | +              | 0         | —              | 0                | +1                                |

## Supplementary Reference

- 1 Henderson, R. K. *et al.* Expanding GSK's solvent selection guide—embedding sustainability into solvent selection starting at medicinal chemistry. *Green Chem.* **13**, 854-862 (2011).
- 2 Lindahl, A., Hess, van der Spoel. GROMACS 2020.4 Source code: Zenodo. (2020). <https://doi.org/doi.org/10.5281/zenodo.4054979>
- 3 Dodda, L. S., Cabeza de Vaca, I., Tirado-Rives, J. & Jorgensen, W. L. LigParGen web server: an automatic OPLS-AA parameter generator for organic ligands. *Nucleic Acids Res.* **45**, W331-W336 (2017).
- 4 Canongia Lopes, J. N. & Pádua, A. A. Molecular force field for ionic liquids III: Imidazolium, pyridinium, and phosphonium cations; chloride, bromide, and dicyanamide anions. *J. Phys. Chem. B* **110**, 19586-19592 (2006).
- 5 Abascal, J. L. & Vega, C. A general purpose model for the condensed phases of water: TIP4P/2005. *J. Chem. Phys.* **123** (2005).
- 6 Zeron, I., Abascal, J. & Vega, C. A force field of  $\text{Li}^+$ ,  $\text{Na}^+$ ,  $\text{K}^+$ ,  $\text{Mg}^{2+}$ ,  $\text{Ca}^{2+}$ ,  $\text{Cl}^-$ , and  $\text{SO}_4^{2-}$  in aqueous solution based on the TIP4P/2005 water model and scaled charges for the ions. *J. Chem. Phys.* **151** (2019).
- 7 Lim, J.-M. *et al.* Intrinsic origins of crack generation in Ni-rich  $\text{LiNi}_{0.8}\text{Co}_{0.1}\text{Mn}_{0.1}\text{O}_2$  layered oxide cathode material. *Sci. Rep.* **7**, 39669 (2017).
- 8 Fisher, C. A., Hart Prieto, V. M. & Islam, M. S. Lithium battery materials  $\text{LiMPO}_4$  (M = Mn, Fe, Co, and Ni): insights into defect association, transport mechanisms, and doping behavior. *Chem. Mater.* **20**, 5907-5915 (2008).
- 9 Lim, T.-C. Alignment of Buckingham parameters to generalized Lennard-Jones potential functions. *Z. Naturforsch. A* **64**, 200-204 (2009).
- 10 Sanville, E., Kenny, S. D., Smith, R. & Henkelman, G. Improved grid-based algorithm for Bader charge allocation. *J. Comput. Chem.* **28**, 899-908 (2007).

- 11 Kresse, G. & Hafner, J. Ab initio molecular dynamics for liquid metals. *Phys. Rev. B* **47**, 558 (1993).
- 12 Perdew, J. P., Burke, K. & Ernzerhof, M. Generalized gradient approximation made simple. *Phys. Rev. Lett.* **77**, 3865 (1996).
- 13 Oh, H. *et al.* Anion-Induced Interfacial Liquid Layers on LiCoO<sub>2</sub> in Salt-in-Water Lithium-Ion Batteries. *JACS Au* **3**, 1392-1402 (2023).
- 14 Dienwiebel, I. *et al.* Enabling Aqueous Processing for LiNi<sub>0.5</sub>Mn<sub>1.5</sub>O<sub>4</sub>-Based Positive Electrodes in Lithium-Ion Batteries by Applying Lithium-Based Processing Additives. *Adv. Energy Sustain. Res.* **2**, 2100075 (2021).
- 15 Dubouis, N. *et al.* The role of the hydrogen evolution reaction in the solid–electrolyte interphase formation mechanism for “Water-in-Salt” electrolytes. *Energy Environ. Sci.* **11**, 3491-3499 (2018).
- 16 Ogihara, N. *et al.* Theoretical and Experimental Analysis of Porous Electrodes for Lithium-Ion Batteries by Electrochemical Impedance Spectroscopy Using a Symmetric Cell. *J. Electrochem. Soc.* **159**, A1034-A1039 (2012).
- 17 H. Sun, L. M. Three-dimensional holey-graphene/niobia composite architectures for ultrahigh-rate energy storage. *Science* **356**, 599 (2017).
- 18 Haydary, J. *Chemical process design and simulation: Aspen Plus and Aspen Hysys applications.* (John Wiley & Sons, 2019).
- 19 Akula, P., Lee, A., Eslick, J., Bhattacharyya, D. & Miller, D. C. J. A. J. A modified electrolyte non-random two-liquid model with analytical expression for excess enthalpy: Application to the MEA-H<sub>2</sub>O-CO<sub>2</sub> system. *AIChE J.* **69**, e17935 (2023).
- 20 Ahmed, S., Nelson, P. A., Gallagher, K. G. & Dees, D. W. J. J. o. P. S. Energy impact of cathode drying and solvent recovery during lithium-ion battery manufacturing. *J. Power Sources* **322**, 169-178 (2016).

- 21 Turton, R., Bailie, R. C., Whiting, W. B. & Shaeiwitz, J. A. *Analysis, synthesis and design of chemical processes*. (Pearson Education, 2008).
- 22 Wood, M. *et al.* Chemical stability and long-term cell performance of low-cobalt, Ni-Rich cathodes prepared by aqueous processing for high-energy Li-Ion batteries. *Energy Stor. Mater.* **24**, 188-197 (2020).
- 23 Radloff, S., Scurtu, R.-G., Hölzle, M. & Wohlfahrt-Mehrens, M. Applying established water-based binders to aqueous processing of  $\text{LiNi}_{0.83}\text{Co}_{0.12}\text{Mn}_{0.05}\text{O}_2$  positive electrodes. *J. Electrochem. Soc.* **168**, 100506 (2021).
- 24 Radloff, S., Scurtu, R.-G., Hölzle, M. & Wohlfahrt-Mehrens, M. Water-based  $\text{LiNi}_{0.83}\text{Co}_{0.12}\text{Mn}_{0.05}\text{O}_2$  electrodes with excellent cycling stability fabricated using unconventional binders. *J. Electrochem. Soc.* **169**, 040514 (2022).
- 25 Radloff, S., Scurtu, R.-G., Hölzle, M. & Wohlfahrt-Mehrens, M. Applying established water-based binders to aqueous processing of  $\text{LiNi}_{0.83}\text{Co}_{0.12}\text{Mn}_{0.05}\text{O}_2$  positive electrodes. *J. Electrochem. Soc.* **168**, 100506 (2021).
- 26 Heidbüchel, M. *et al.* Enabling Aqueous Processing of Ni-Rich Layered Oxide Cathode Materials by Addition of Lithium Sulfate. *ChemSusChem* **16**, e202202161 (2023).
- 27 Kuo, J.-H. & Li, C.-C. Water-based process to the preparation of nickel-rich  $\text{Li}(\text{Ni}_{0.8}\text{Co}_{0.1}\text{Mn}_{0.1})\text{O}_2$  cathode. *J. Electrochem. Soc.* **167**, 100504 (2020).
- 28 Radloff, S., Scurtu, R.-G., Hölzle, M. & Wohlfahrt-Mehrens, M. Water-based  $\text{LiNi}_{0.83}\text{Co}_{0.12}\text{Mn}_{0.05}\text{O}_2$  electrodes with excellent cycling stability fabricated using unconventional binders. *J. Electrochem. Soc.* **169**, 040514 (2022).
- 29 Hofmann, M., Kapuschinski, M., Guntow, U. & Giffin, G. A. Implications of aqueous processing for high energy density cathode materials: part I. Ni-rich layered oxides. *J. Electrochem. Soc.* **167**, 140512 (2020).
- 30 Ibing, L. *et al.* The role of the pH value in water-based pastes on the processing and

- performance of Ni-rich  $\text{LiNi}_{0.5}\text{Mn}_{0.3}\text{Co}_{0.2}\text{O}_2$  based positive electrodes. *J. Power Sources* **475**, 228608 (2020).
- 31 Chen, Z. *et al.* Toward greener lithium-ion batteries: Aqueous binder-based  $\text{LiNi}_{0.4}\text{Co}_{0.2}\text{Mn}_{0.4}\text{O}_2$  cathode material with superior electrochemical performance. *J. Power Sources* **372**, 180-187 (2017).
- 32 Loeffler, N. *et al.* Performance of  $\text{LiNi}_{1/3}\text{Mn}_{1/3}\text{Co}_{1/3}\text{O}_2$ /graphite batteries based on aqueous binder. *J. Power Sources* **248**, 915-922 (2014).
- 33 Loeffler, N. *et al.* In situ coating of  $\text{Li}[\text{Ni}_{0.33}\text{Mn}_{0.33}\text{Co}_{0.33}]\text{O}_2$  particles to enable aqueous electrode processing. *ChemSusChem* **9**, 1112-1117 (2016).
- 34 Hofmann, M., Nagler, F., Guntow, U., Sextl, G. & Giffin, G. A. Long-term cycling performance of aqueous processed Ni-rich  $\text{LiNi}_{0.8}\text{Co}_{0.15}\text{Al}_{0.05}\text{O}_2$  cathodes. *J. Electrochem. Soc.* **168**, 060511 (2021).
- 35 Li, J., Armstrong, B. L., Kiggans, J., Daniel, C. & Wood, D. L. Lithium ion cell performance enhancement using aqueous  $\text{LiFePO}_4$  cathode dispersions and polyethyleneimine dispersant. *J. Electrochem. Soc.* **160**, A201 (2012).
- 36 Porcher, W., Lestriez, B., Jouanneau, S. & Guyomard, D. Optimizing the surfactant for the aqueous processing of  $\text{LiFePO}_4$  composite electrodes. *J. Power Sources* **195**, 2835-2843 (2010).
- 37 Li, C.-C., Lee, J.-T., Lo, C.-Y. & Wu, M.-S. Effects of PAA-NH<sub>4</sub> addition on the dispersion property of aqueous  $\text{LiCoO}_2$  slurries and the cell performance of as-prepared  $\text{LiCoO}_2$  cathodes. *Electrochem. Solid-State. Lett.* **8**, A509 (2005).
- 38 Lux, S., Schappacher, F., Balducci, A., Passerini, S. & Winter, M. Low cost, environmentally benign binders for lithium-ion batteries. *J. Electrochem. Soc.* **157**, A320 (2010).
- 39 Ye, R., Hamzelui, N., Ihrig, M., Finsterbusch, M. & Figgemeier, E. Water-Based Fabrication of a  $\text{Li}|\text{Li}_7\text{La}_3\text{Zr}_2\text{O}_{12}|\text{LiFePO}_4$  Solid-State Battery— Toward Green Battery Production. *ACS Sustain. Chem. Eng.* **10**, 7613-7624 (2022).



- 40 Ryou, M.-H., Hong, S., Winter, M., Lee, H. & Choi, J. W. Improved cycle lives of  $\text{LiMn}_2\text{O}_4$  cathodes in lithium ion batteries by an alginate biopolymer from seaweed. *J. Mater. Chem. A* **1**, 15224-15229 (2013).
- 41 Byrne, F. P. *et al.* Tools and techniques for solvent selection: green solvent selection guides. *Sustain. Chem. Process.* **4**, 1-24 (2016).
- 42 Bresser, D., Buchholz, D., Moretti, A., Varzi, A. & Passerini, S. Alternative binders for sustainable electrochemical energy storage—the transition to aqueous electrode processing and bio-derived polymers. *Energy Environ. Sci.* **11**, 3096-3127 (2018).